Role of layer order on the equi-biaxial behavior of Al/Mo bilayers

M.J. Cordill, P. Kreiml, B. Putz, C. Mitterer, D. Thiaudière, C. Mocuta, P.-O. Renault, D. Faurie

Role of layer order on the equi-biaxial behavior of Al/Mo bilayers

M.J. Cordill[a,b*], P. Kreiml[b], B. Putz[c], C. Mitterer[b], D. Thiaudière[d], C. Mocuta[d], P.-O. Renault[e], D. Faurie[f]

[a]Erich Schmid Institute of Materials Science, Austrian Academy of Sciences, Jahnstrasse 12, 8700 Leoben, Austria
[b]Department of Materials Science, Montanuniversität Leoben, Franz-Josef-Strasse 18, 8700 Leoben, Austria
[c]Empa, Swiss Federal Laboratories for Materials Science and Technology, Feuerwerkerstrasse 39, 3602 Thun, Switzerland
[d]Synchrotron SOLEIL, L'Orme des Merisiers, Saint-Aubin, BP 48, 91192 Gif-sur-Yvette Cedex, France
[e]Pprime Institute, CNRS-University of Poitiers, Departement de Physique et Mecanique des Materiaux, 11 Bd Pierre et Marie Curie TSA 41123, 86073 Poitiers Cedex 9, France
[f]LSPM-CNRS, UPR3407, Université Sorbonne Paris Nord, 93430 Villetaneuse, France

*corresponding author: megan.cordill@oeaw.ac.at

Abstract

Thin film architectures with brittle and ductile material layers are often combined for functionality. Easy to fracture brittle films are often necessary due to their function as diffusion barriers, adhesion or protective layers. Especially in the field of flexible and wearable electronics brittle materials may cause short lifetimes. Direct current magnetron sputtered bilayers on a polyimide substrate containing brittle Mo and ductile Al layers (Al/Mo/PI and Mo/Al/PI) as well as Al films (Al/PI) were subjected to equi-biaxial loading with in-situ X-ray diffraction measurements. The setup enabled the extraction of the stress and full width at half-maximum as a function of the strain. The data yields deeper insights into underlying deformation and fracture mechanisms and the significance of the layer arrangement. It will be demonstrated that for stretchable applications the position of the Mo layer affects the fracture strain of the bilayers and the individual layers.

Keywords

Sputtering, X-ray, multilayer thin films, interfaces, in-situ biaxial

Metal thin films supported by polymer substrates have applications in flexible electronics, foldable displays and even in space exploration. The most common method to evaluate such thin film systems is uniaxial straining to induce cracking and sometimes delamination of the films. While uniaxial testing does have significant merit, biaxial straining is more suited to the material system's application load. Furthermore, when combined with in-situ X-ray diffraction (XRD) [1–3] multilayer film architectures can be examined more thoroughly by providing vital information about the mechanical behavior of different metals in multilayer nanolaminates [4,5]. Of further interest is to examine how the layer order of a simple bilayer system affects the mechanical behavior. It has already been demonstrated that the addition of brittle adhesion or protective films generally leads to an embrittlement of a normally ductile film compared to single ductile films under uniaxial loading [6–9]. However, only few studies investigated the mechanical behavior of material systems, such as Au, Ni, and W/Cu, under biaxial loading conditions [2,3,10,11].

Al/Mo bi- and trilayers are currently used as electrodes in many display applications [12–14]. Here, a bilayer system of Al/Mo will be compared to a single layer of Al. It will be demonstrated that the placement of the brittle Mo film in the Al/Mo bilayer architecture strongly influences the mechanical behavior of the bilayer. The study of the interface order in the bilayer system leading to multilayer nanolaminates will help design better and more robust nanolaminates for various applications ranging from flexible electronics, wear resistance, and even radiation protection [4,15–19]. Indeed, in the case of two-layer systems deposited on a polymer substrate, the differences in behavior can be very significant. On the one hand, the adhesion energy with the polymer necessarily depends on the metal in contact with the polymer [5,20]. On the other hand, the mechanical contrast between the two layers has a major importance on the overall behavior. Indeed, in the case of a very thin bilayer as compared to the thickness of the substrate, which loads the whole system above it, the continuity of the

displacements at the successive interfaces (on the global and local scale) is the key phenomenon. The polycrystalline nature of these layers (showing nanograins) should result in strain heterogeneities that would be different depending on whether the interface with the substrate is with a brittle or ductile layer. Indeed plasticity induces intra- and intergranular heterogeneities at the nanoscale [21], while cracking of a brittle layer induces heterogeneities less related to the microstructure but more to the crack density [22]. Thus, it is likely that the order of deposition between a rigid/brittle layer and a less rigid and ductile layer will affect the strain distribution. Both phenomena can be probed by the in-situ study of X-ray stress and full width at half-maximum FWHM (see references [23] and [3], respectively).

Therefore, the aim of the paper is to elucidate the influence of the layer order on these strain heterogeneities and thus to the whole mechanical behavior in biaxial loading. Single and bilayers of Al and Mo films were deposited onto 50 μm thick Upilex-S polyimide (PI) foils using direct current (DC) magnetron sputtering. The substrates were pre-cut into cruciform shapes similar to Ref. [2] using 16 mm wide arms. Films were deposited using an industrial scale magnetron sputter system (FHR.Line.600-V) equipped with a planar Al target (600 × 125 mm) and a rotary Mo target (Ø 125 × 600 mm) using an Ar flow rate of 300 sccm, corresponding to a pressure of 0.53 Pa. For the 250 nm Al films, a DC power of 3.5 kW and deposition time of 70 seconds was used. The 50 nm Mo films were deposited with a DC power of 4.5 kW and deposition time of 9.5 seconds. To avoid edge effects [1] the films were partly etched away after deposition, leaving only undamaged circles of the thin films (diameter ~1.5 cm) in the center of each cruciform for testing. Two bilayer architectures were created, namely Al/Mo and Mo/Al. The two bilayers and a 250 nm Al single film were equi-biaxially strained to about 3% at the DiffAbs beam line at the synchrotron radiation facility SOLEIL [10], following a similar procedure as in Ref. [3]. With the incident angle and XPAD detection angle fixed, a hybrid pixel area detection was used to obtain a full intensity versus 2-theta curve simultaneously.

Additionally, the instrument resolution was evaluated to be 0.05 degrees and the correction of the FWHM does not significantly change the reported values. Before straining the surface roughness of all samples were measured with atomic force microscopy (AFM, DI 3100) and found to be in the range of 15 nm to 17 nm. After straining examined with scanning electron microscopy (SEM, Zeiss LEO 1525) and focused ion beam (FIB, Zeiss LEO 1540XB workstation) cross-sections.

Equi-biaxial straining of the single Al and the Al/Mo and Mo/Al bilayer films illustrated how the architecture of the layers influences the mechanical behavior. Starting with the single 250 nm Al film (Figure 1a), four different domains of mechanical behavior are observed in the stress and FWHM data. The FWHM provides information about the lattice defect density and strain heterogeneities through peak broadening and helps to determine the different regions with film stresses [24,25]. Domain I is the elastic behavior (linear stress increase, constant FWHM) and is followed by Domain II, micro-plasticity, when dislocations are activated in the Al film. Domain II is defined as a continued increase to bending over of the stress behavior and an increase of FWHM and is specific to the Al film (a different mechanism is present in Mo since it behaves brittle [26]). In the next region, Domain III, the stress level slightly decreases while FWHM continues to increase with a lower rate compared to II. Domain III is characterized by localized plastic deformation, more commonly known as necking and is a characteristic deformation mechanism of ductile thin films on polymers [6,27]. Finally, Domain IV exemplifies the through thickness cracking behavior resulting in clear stress relaxation and constant FWHM. The sudden drops in film stress and FWHM at 3% stem from instrumentation and are not characteristics of film deformation. The observed domains are similar to those noted by Faurie, et al. [3] for biaxial straining of Ni films with the difference that for Al the necking and fragmentation domains are observed as two clearly separate regimes. For the Ni films in

Ref. [3] no stress plateau is observed, possibly because of the reduced film thickness of only 50 nm.

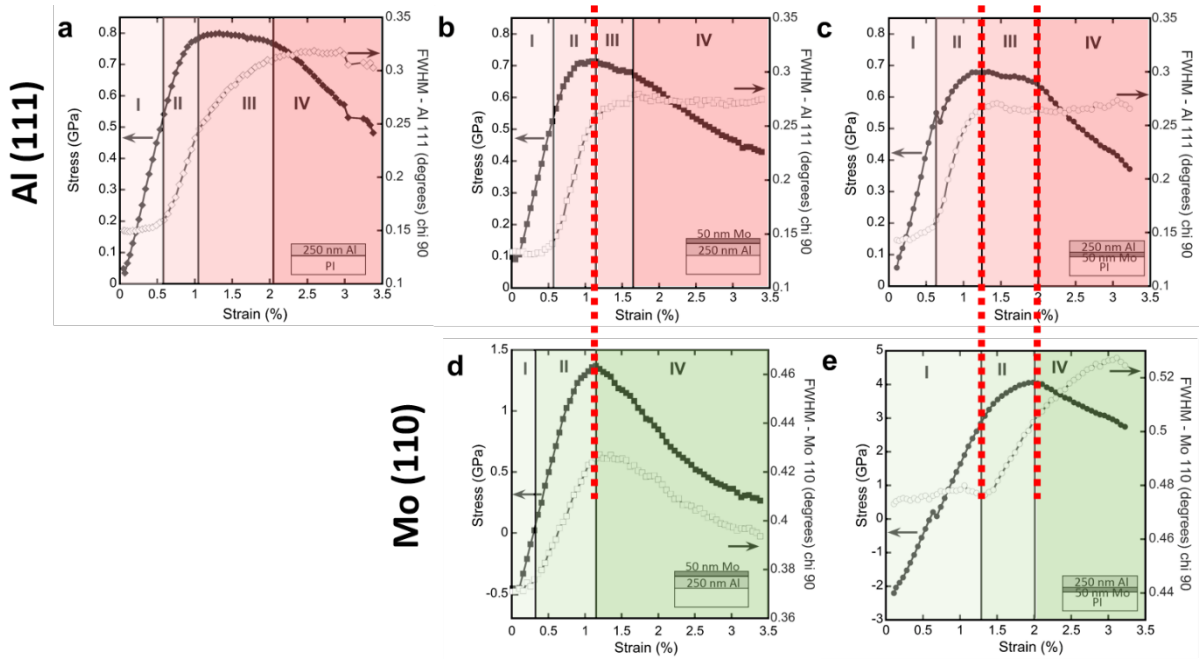

Figure 1: Al and Mo film stresses and FWHM measured from in-situ XRD equi-biaxial straining experiments illustrating the deformation domains (I: Elastic, II: Micro-Plasticity (Al) or Strain Heterogeneities (Mo), III: Necking, and IV: Fragmentation). (a) Al 111 peak of the Al/PI, (b) Al 111 peak of the Mo/Al/PI, (c) Al 111 peak of the Al/Mo/PI, (d) Mo 110 peak of the Mo/Al/PI, and (e) Mo 110 peak of the Al/Mo/PI. The red dashed lines through (b-d) and (c-e) illustrate where the transition between different deformation regimes converges for Al and Mo.

The same four mechanisms are observed in the Al layers of the Mo/Al/PI bilayer (Figure 1b) and the Al/Mo/PI bilayer (Figure 1c). The onset of early plastic deformation in the Al films in the bilayers (Domain II: Micro-Plasticity) occurs at similar stress levels as the single Al film. The influence of the Mo layer on Al deformation in the bilayer systems becomes apparent in Domain III, depending on whether the Al film is on the PI substrate (Figure 1b) or on the Mo (Figure 1c). For Mo/Al/PI the stress decreases and the FWHM increases similar to the single Al film (Figure 1a), but Domain III ends at lower applied strains. When Al is on Mo (Figure 1c) the FWHM remains constant, indicating reduced plasticity and dislocation activity.

Different FWHM trends in Domain III depending on the layer order evidence that the bilayer order influences the mechanical response of multilayers. After necking (Domain III), fragmentation (Domain IV) is observed in both bilayers as a pronounced decrease in the measured stress and constant FWHM values.

In the Mo layers only three domains are observed (Figure 1d,e). For both bilayers, elastic behavior (Domain I) is followed by Domain II, then fragmentation and stress relaxation (Domain IV). In the bcc Mo film, plasticity is difficult to initiate, thus the FWHM increase in Domain II for Mo is defined by increasing strain heterogeneities induced via the Al-Mo interface rather than micro-plasticity present in Al films. The different Domain II mechanisms will be further discussed later. In contrast to Al fragmentation, the FWHM of Mo increases when Mo is directly deposited onto PI (Figure 1e) and decreases when Mo is above Al (Figure 1d). For the Al/Mo/PI system, the onset of Domain II in the Mo layer coincides with necking (Domain III) in the Al and later on both layers fragment simultaneously (compare Figure 1c and e, red lines). When Mo is a top coating (Figure 1d), the elastic region is extremely reduced compared to the case when Mo is an interlayer and an almost instant increase in FWHM is observed upon straining (Domain II). This Mo Domain II is followed by Mo fragmentation (Domain IV) as revealed by stress relaxation. In this configuration (Mo/Al/PI), the onset of Mo fragmentation coincides with the onset of necking in Al (red line between Figure 1b and 1d) and appears before Al fragments indicating a mutual influence of the two layers. This behavior has been previously shown for the Inconel/Ag/Teflon system [7], and is noteworthy because the brittle layer fragmentation also occurs at lower applied strains. The FWHM behavior is different in the brittle Mo films, where it either continued to increase in Domain IV (Figure 1e) or decrease (Figure 1d). The difference depends on the position of the Mo layer as an interlayer or top layer and the opposite behavior of the Mo FWHM is not yet understood.

Further examination of the FWHM curves helps to identify and distinguish the different deformation mechanisms of Al and Mo in Domain II. In both cases, Domain II is characterized by an initially linear increasing film stress and a first-time increase of the FWHM from the initial plateau value. However, the relative variation of FWHM in the Mo films is rather small compared to the relative variation of FWHM found in the Al films (Figure 2). For all three Al films, FWHM increases from approximately 0.15° to about 0.25° within Domain II, making the relative increase 70%. In contrast, the increase of FWHM of Mo is only from 0.48° up to 0.5° for Al/Mo/PI and from 0.37° up to 0.42° for Mo/Al/PI. This different magnitude of FWHM increase is an indication that different physical mechanisms, namely micro-plasticity (Al) and strain heterogeneities (Mo), are present in Domain II during equi-biaxial straining, whereby micro-plasticity causes a larger FWHM increase compared to strain heterogeneities. Regarding strain heterogeneities in the Mo layers, the two different bilayer geometries need to be considered separately. In the case of the Mo interlayer, localized necking of the overlying Al film (Figure 1c-e, red line) is transmitted at/via the Al-Mo interface inducing strain heterogeneities in Mo. The situation is slightly different for the Mo overcoat being strained by the underlying Al film. The very early increase of FWHM in Figure 1b-d can be explained by (i) an increased roughness of the Mo/Al interface compared to Mo/PI, (ii) the difference in residual stresses of Mo layers (-0.5 GPa vs. -2 GPa), and (iii) micro-plasticity in Al, creating strain heterogeneities in the Al film, which are in turn transmitted to Mo at the interface. The associated FWHM increase (14%) is higher compared to the interlayer case (4%).

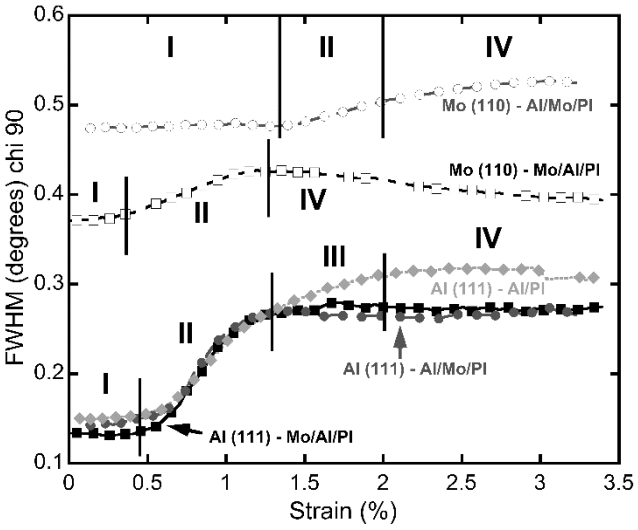

Figure 2: Comparison of the FWHM values for Al 111 and Mo 110 for all film systems. The difference in the relative FWHM increase indicates that two different physical mechanisms are activated in Domain II for the Al (micro-plasticity) and Mo (strain heterogeneities). The approximate domains I-IV are also indicated.

During the final stage of fragmentation under equi-biaxial loading (Domain IV), the formation of through thickness cracks reduces the average stress measured in all layers and has been observed in other in-situ XRD experiments [6,7,28]. Post-mortem SEM micrographs (Figure 3) of the samples also show that through thickness cracking occurred. The fragmentation of the Al single film (Figure 3a) is difficult to observe due the surface roughness and relaxation of the PI substrate, which closes cracks that may have formed [29,30]. However, the XRD data clearly indicate stress relaxation by through thickness cracking. The cross-sections of the bilayers (Figure 3b,c) showcase that cracks in the Mo layers directly correlate to cracks in the Al film, regardless of the layer order. The correlation of the Al and Mo cracks has been observed before for uniaxial tensile straining of Al/Mo bilayers of different thicknesses [9]. Another feature of biaxial straining is the mud crack pattern, best visible in Figure 3d. Through thickness cracks were observed when the Mo was on top of the Al layer and necking is more pronounced with Mo as the interlayer. The stress data also illustrate that the necking regime is longer when Mo is an interlayer between Al and PI.

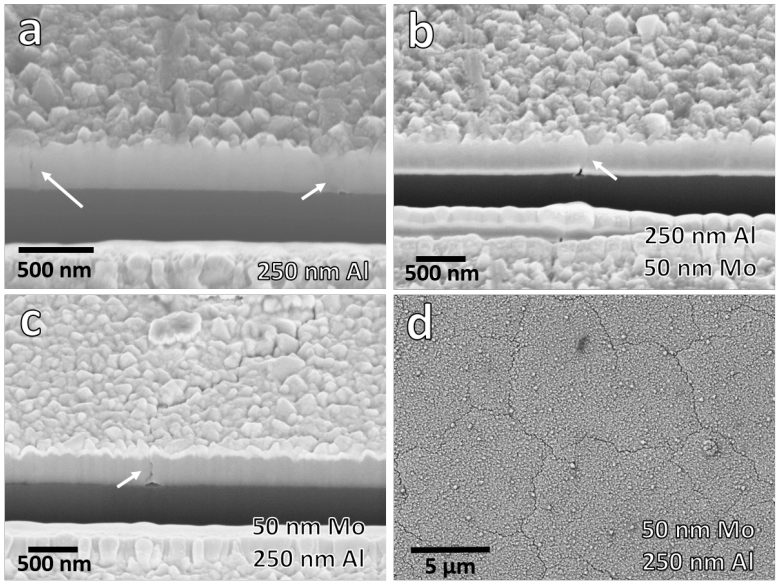

Figure 3: SEM micrographs after equi-biaxial straining of (a) 250 nm Al, (b) 250 nm Al/50 nm Mo/PI, (c) 50 nm Mo/250 nm Al/PI, and (d) Mo/Al/PI evidencing mud crack pattern on the surface. Arrows in indicate through thickness cracks or closed necks.

The film architecture did not substantially influence measured stresses in the Al layers. For all three Al layers, maximum stresses of 0.7-0.8 GPa were reached slightly above 1% applied strain which corresponds to the transition from Domain II to Domain III in Al. The similar maximum stresses indicate similar microstructures in the Al films. At this same strain, the Mo layers transition from Domain I to Domain II or Domain II to Domain IV, depending on the layer order. Fragmentation of the Al layers occurs between strains of 1.6-2.0%, which is the same strain range where fracture of Mo was observed. Compared to Al, the Mo layers reach higher maximum stresses under equi-biaxial loading, which can be equated to the fracture stresses due to the absence of Domain III. The Mo interlayer achieved the highest maximum stress of about 4 GPa at 2% applied strain. This strain also corresponds to the end of the necking domain and the beginning of the fragmentation domain for the overlying Al film (Figure 1b,d). For the Mo/Al/PI bilayer system, the Mo layer reaches a maximum stress of only 1.4 GPa at about 1.2% applied strain, which corresponds to the end of micro-plasticity and the beginning

of the necking domain in the underlying Al film (Figure 1b,d). The lower strain value as compared to the Mo interlayer configuration can partly be due to the different residual stress state (-0.5 GPa vs. -2 GPa), whereby compressive residual stresses shift fracture to higher applied strains [26]. The Mo/Al/PI bilayer has the lowest Mo fracture stress and fracture of Mo and Al occurred at lower strains compared to the other film systems which were equi-biaxially strained. These comparisons further demonstrate that film architecture has a significant influence on the mechanical behavior.

Equi-biaxial straining with in-situ XRD measurements of different single and bilayer thin film architectures of Al and Mo was performed. These experiments revealed that the ductile Al films go through four domains of mechanical behavior while the brittle Mo films only exhibit three domains. Comparing the biaxially strained film systems, it was shown that Mo interlayers can reach higher maximum stresses compared to when the same Mo layer is placed on top of the Al film of the same thickness. Unexpectedly, similar maximum stresses and FWHM values were observed in all Al layers of the same thickness in the different architectures. The results presented here illustrate that multilayer film architectures greatly influence the mechanical behavior and brittle top layers in bilayer systems with ductile and brittle components are worse for both layers compared to using a brittle interlayer.

SOLEIL is gratefully acknowledged for the beam time allocation (Proposal 20190179). This work was in part supported by the Austrian Research Promotion Agency (FFG) within the framework of the project E2 SPUTTERTECH PLUS (project number 857043) and was also supported by the French Government Program “Investissements d'Avenir” (LABEX INTER-ACTIFS, reference ANR-11-LABX-0017-01). B.P. acknowledges support from the EMPAPOSTDOCS-II program, which received funding from the European Union’s Horizon 2020 research and innovation program under the Marie Skłodowska-Curie grant agreement

number 754364. K.H. Pichler from the Montanuniversität Leoben is also acknowledged for helping to deposit the samples.

References

[1] S. Djaziri, P.-O. Renault, F. Hild, E. Le Bourhis, P. Goudeau, D. Thiaudière, D. Faurie, J. Appl. Crystallogr. 44 (2011) 1071–1079.

[2] G. Geandier, D. Faurie, P.O. Renault, D. Thiaudière, E. Le Bourhis, J. Appl. Crystallogr. 47 (2014) 181–187.

[3] D. Faurie, F. Zighem, P. Godard, G. Parry, T. Sadat, D. Thiaudière, P.-O. Renault, Acta Mater. 165 (2019) 177–182.

[4] M.N. Polyakov, J. Lohmiller, P.A. Gruber, A.M. Hodge, Adv. Eng. Mater. 17 (2015) 810–814.

[5] M.J. Cordill, A. Kleinbichler, B. Völker, P. Kraker, D.R. Economy, D. Többens, C. Kirchlechner, M.S. Kennedy, Mater. Sci. Eng. A 735 (2018) 456–462.

[6] V.M. Marx, F. Toth, A. Wiesinger, J. Berger, C. Kirchlechner, M.J. Cordill, F.D. Fischer, F.G. Rammerstorfer, G. Dehm, Acta Mater. 89 (2015) 278–289.

[7] B. Putz, C. May-Miller, V. Matl, B. Völker, D.M. Többens, C. Semprimoschnig, M.J. Cordill, Scr. Mater. 145 (2018) 5–8.

[8] B. Putz, R.L. Schoeppner, O. Glushko, D.F. Bahr, M.J. Cordill, Scr. Mater. 102 (2015) 23–26.

[9] P. Kreiml, M. Rausch, V.L. Terziyska, H. Köstenbauer, J. Winkler, C. Mitterer, M.J. Cordill, Thin Solid Films 665 (2018) 131–136.

[10] S. Djaziri, D. Faurie, P.O. Renault, E. Le Bourhis, P. Goudeau, G. Geandier, D. Thiaudière, Acta Mater. 61 (2013) 5067–5077.

[11] P. Godard, D. Faurie, P.O. Renault, J. Appl. Phys. 127 (2020).

[12] B.-K. Kim, H.-S. Park, J.-H. Choung, S.-Y. Hong, L. Ji-Sun, B.-J. Lee, K.-J. Baek, T.-H. Rhee, Y.-S. Song, Etchant Composition, Patterning Conductive Layer and Manufacturing Flat Panel, Display Device Using the Same, US Patent 7,985,982, 2011.

[13] J.A. Cunningham, C.R. Fuller, R.C. Hooper, R.H. Wakefield, METALLIZATION SYSTEM FOR SEMCONDUCTORS, US Patent 3,654,526, 1972.

[14] K. Onisawa, S. Takayama, Y. Shigesato, T. Takahashi, Thin Film Transistors, Springer US, Boston, MA, 2004.

[15] P.A. Gruber, J. Böhm, F. Onuseit, A. Wanner, R. Spolenak, E. Arzt, Acta Mater. 56 (2008) 2318–2335.

[16] P.A. Gruber, C. Solenthaler, E. Arzt, R. Spolenak, Acta Mater. 56 (2008) 1876–1889.

[17] W. He, M. Han, P. Goudeau, E. Le Bourhis, P.O. Renault, S. Wang, L. an Li, Appl. Surf. Sci. 434 (2018) 771–780.

[18] C.C. Aydiner, D.W. Brown, N.A. Mara, J. Almer, A. Misra, Appl. Phys. Lett. 94 (2009) 10–13.

[19] N.A. Mara, D. Bhattacharyya, R.G. Hoagland, A. Misra, Scr. Mater. 58 (2008) 874–877.

[20] B. Putz, B. Völker, C. Semprimoschnig, M.J. Cordill, Microelectron. Eng. 167 (2017) 17–22.

[21] S. Van Petegem, L. Li, P.M. Anderson, H. Van Swygenhoven, Thin Solid Films 530

(2013) 20–24.

[22] I. Ben Cheikh, G. Parry, D. Dalmas, R. Estevez, J. Marthelot, Int. J. Solids Struct. 180–181 (2019) 176–188.

[23] D.S. Gianola, S. Van Petegem, M. Legros, S. Brandstetter, H. Van Swygenhoven, K.J. Hemker, Acta Mater. 54 (2006) 2253–2263.

[24] M. Vashista, S. Paul, Philos. Mag. 92 (2012) 4194–4204.

[25] I.C. Noyan, J.B. Cohen, Residual Stress: Measurement by Diffraction and Interpretation, Springer-Verlag New York, New York, 1987.

[26] T. Jörg, M.J. Cordill, R. Franz, C. Kirchlechner, D.M. Többens, J. Winkler, C. Mitterer, Mater. Sci. Eng. A 697 (2017) 17–23.

[27] J. Berger, O. Glushko, V.M. Marx, C. Kirchlechner, M.J. Cordill, JOM 68 (2016).

[28] B. Putz, O. Glushko, V.M. Marx, C. Kirchlechner, D. Toebbens, M.J. Cordill, MRS Adv. 1 (2016) 773–778.

[29] O. Glushko, V.M. Marx, C. Kirchlechner, I. Zizak, M.J. Cordill, Thin Solid Films 552 (2014) 141–145.

[30] O. Glushko, B. Putz, M.J. Cordill, Thin Solid Films 699 (2020) 137906.